Provided for non-commercial research and education use.
Not for reproduction, distribution or commercial use.

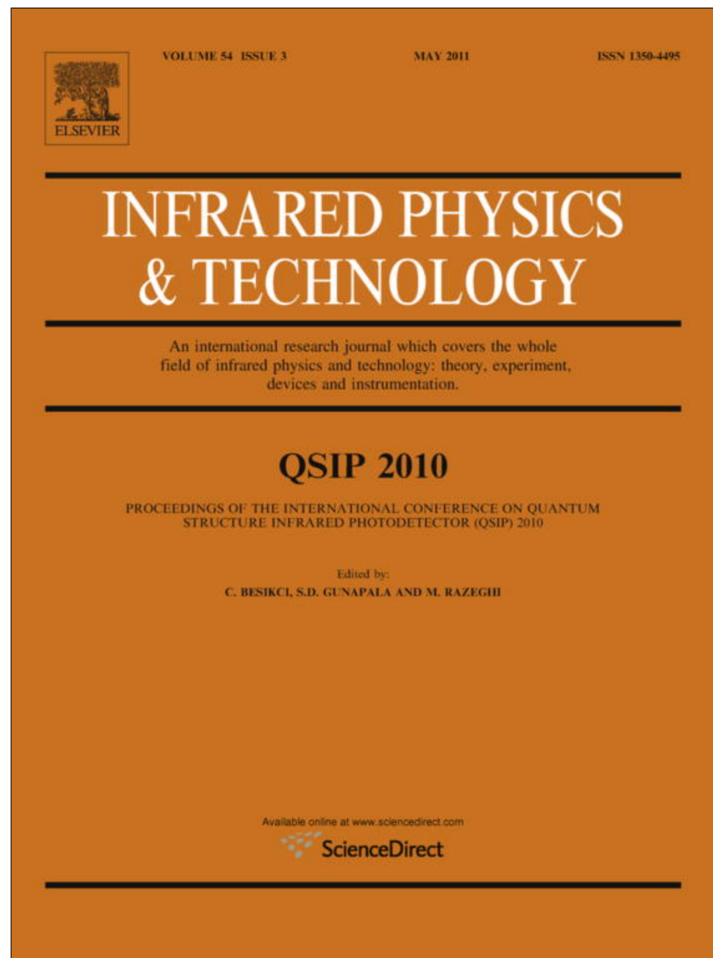

This article appeared in a journal published by Elsevier. The attached copy is furnished to the author for internal non-commercial research and education use, including for instruction at the authors institution and sharing with colleagues.

Other uses, including reproduction and distribution, or selling or licensing copies, or posting to personal, institutional or third party websites are prohibited.

In most cases authors are permitted to post their version of the article (e.g. in Word or Tex form) to their personal website or institutional repository. Authors requiring further information regarding Elsevier's archiving and manuscript policies are encouraged to visit:

http://www.elsevier.com/copyright

Author's personal copy

Infrared Physics & Technology 54 (2011) 296–301

Contents lists available at ScienceDirect

Infrared Physics & Technology

journal homepage: www.elsevier.com/locate/infrared

Effects of graded barriers on the operation of split-off band infrared detectors

A.G.U. Perera [a,*], S.G. Matsik [a], D.P. Pitigala [a], Y.F. Lao [a], S.P. Khanna [b], L.H. Li [b], E.H. Linfield [b], Z.R. Wasilewski [c], M. Buchanan [c], X.H. Wu [c], H.C. Liu [c]

[a] Department of Physics and Astronomy, Georgia State University, Atlanta, GA 30303, USA
[b] School of Electronic and Electrical Engineering, University of Leeds, Leeds LS2 9JT, UK
[c] Institute for Microstructural Sciences, National Research Council, Ottawa, Canada K1A 0R6

ARTICLE INFO

Article history:
Available online 25 December 2010

Keywords:
Infrared
Graded barrier
High temperature

ABSTRACT

Increasing the operating temperature of infrared detectors is a prime importance for practical applications. The use of split-off band transitions has been proposed for high operating temperature infrared detectors. Initial results showed increasing the potential barrier for free carrier emission has led to increases in operating temperature from 150 K for a detector with an 8 μm threshold to room temperature for detector with a 4 μm threshold. However, these detectors showed a low responsivity due to the capture of carriers in each emitter. A proposal was made to use graded barriers with an offset between the barriers on the two sides of an emitter as a method of reducing the capture in the emitters. Two GaAs/AlGaAs samples with a single graded barrier (Al fraction $x = 0.57$ to 1 and 0.45 to 0.75, respectively) were used to test the effects. The sample with the lower barrier show responsivity increased by a factor of ∼10 or more compared to the higher graded barrier sample and detectors without the graded barrier. The higher graded barrier sample, space charge build up causes almost all potential drop across the first barrier, and hence reduces the response. Based on the modeling it is believed that this effect will be greatly reduced in detectors with multiple periods of graded barriers and emitters, allowing the full gain effects of the graded barriers to be realized.

© 2010 Elsevier B.V. All rights reserved.

1. Introduction

Low temperature cooling required for suppressing the thermal generation processes that cause reduced signal to noise ratio is a key limitation on the successful use of IR detectors in many practical areas. IR detectors operating without cryogenic aid or with reduced cooling requirements will find immense applications in diverse areas including, defense, security, data communication, biomolecular identification, and astronomy. A number of different approaches to improve the operating temperature of IR detectors have been studied, including: HgCdTe, quantum well, quantum dot [1], and type-II strained superlattice detectors [2]. Another improvement is the split-off band detectors, successfully tested recently with a 4 μm threshold, operating up to room temperature [3]. However, the performance of the split-off band detectors was weak due to excessive recapture of excited carriers in the emitters. A model for the response of the split-off band detectors was proposed suggesting possible improvements in their design and preliminary tests on improvements were performed.

The spin orbit split-off detection mechanism, based on photon absorption through spin split-off transitions in the valence band of the p-doped emitter material, provides a potential alternative for IR detection at high operating temperatures. Split-off band detectors consist of highly p-doped emitters between undoped barriers and operate by photoabsorption in the emitter. One possible approach to improving these detectors is to use a graded barrier with an offset between the barrier heights on opposite sides of an emitter. The inclusion of the graded barrier leads to a decrease in the dark current at low bias voltages due to the need to overcome the offset of the grading. For higher biases, the dark current of a device with graded barriers and one without graded barriers is almost exactly the same if the effective field in the barriers is the same. The primary dark current advantage of the graded barrier is the ability to operate at lower effective fields due to improved sweep out of photoexcited carriers. The extra energy of carriers entering over the high side barrier should reduce the excess trapping leading to photoconductive gain by a mechanism similar to that in QWIPs.

Here, we will discuss our theoretical and experimental investigations of split-off based detectors. The present split-off band based IR detection was initially observed for the 2–3 μm range in GaAs/AlGaAs HEterojunction Interfacial Workfunction Internal Photoemission (HEIWIP) detectors [3], and was then further confirmed using detectors specifically designed for high temperature split-off detection [4] which showed response up to 330 K. The

* Corresponding author. Tel.: +1 404 413 6037; fax: +1 404 413 6025.
E-mail address: uperera@gsu.edu (A.G.U. Perera).

1350-4495/$ - see front matter © 2010 Elsevier B.V. All rights reserved.
doi:10.1016/j.infrared.2010.12.033

Author's personal copy

detection mechanism uses an absorption involving a transition from the light/heavy-hole bands into the split-off hole band of the p-doped emitter layers. The photoexcited carriers must then escape over the band offset at the interface either directly in the split-off band or by scattering into the light/heavy-hole bands. The escaped carriers are then swept out of the active region by an external electric field and collected at the contacts. Split-off band transitions also leads to a longer wavelength response extending over 8 μm [5].

2. Theory

The IR absorption in the emitter layer contains both a direct absorption involving only the photon and the hole, and an indirect absorption involving an additional particle. The contribution of these absorption processes gives the total absorption in the emitter region. If additional absorption mechanisms such as interband, or impurity absorption are present they can also be included using the correct quantum mechanical formulas for the absorption probabilities.

The direct absorption considered for the p-type emitters is from the light or heavy-hole bands to the split-off band. The absorption in a unit cell of volume V for the direct transition is given by [6]

$$R = \frac{2V}{(2\pi)^3}\int d^3k(2\pi\hbar)|\langle nk|H_{\rm int}|n'k'\rangle|^2 f(n,k)[1-f(n',k')]\delta(E'-E-\hbar\omega) \quad (1)$$

where $H_{\rm int}$ is the interaction of the photons with the carriers, n and n' indicate the initial and final bands, and $f(n,k)$ is the occupation of the nth band at wave number k with the matrix elements for $H_{\rm int}$ given by

$$\langle nk|H_{\rm int}|n'k'\rangle = -(eA_0/2m)(\mathbf{a}\cdot\mathbf{p}) \quad (2)$$

Momentum conservation will yield $k' = k$ as the photon momentum should be negligible.

The indirect transition is calculated using second order perturbation theory. The absorption in a unit cell is given by

$$R = \frac{2V^2}{(2\pi)^6}\int d^3k d^3k' S f(k)[1-f(k')] \quad (3)$$

where,

$$S = \frac{2\pi}{\hbar}|\langle n'k'|H_{\rm scat}|nk\rangle|^2|\langle n''k''|H_{\rm int}|n'k'\rangle|^2/(\hbar^2\omega^2)\delta(E'-E-\hbar\omega-\hbar\omega_q) \quad (4)$$

with, $H_{\rm scat}$ Hamiltonian dealing with the scattering mechanisms considered and $f(k)$ is the probability of a carrier having momentum k obtained from the Fermi distribution. The scattering matrix element for acoustic deformation scattering is given by

$$\langle n'k'|H_{\rm scat}|nk\rangle = \varepsilon_{\rm ac}[k_{BT}/2Vc_l]^{1/2} \quad (5)$$

where $\varepsilon_{\rm ac}$ is the acoustic deformation potential constant, k_B is the Boltzmann's constant, T is the lattice temperature, and c_l is the longitudinal elastic constant. For optical deformation scattering, the matrix element is given by

$$\langle n'k'|H_{\rm scat}|nk\rangle = D\left[\left(N+\frac{1}{2}\mp\frac{1}{2}\right)\hbar/2\rho V\omega_0\right]^{1/2} \quad (6)$$

where D is the optical deformation potential constant, ρ is the mass density, and ω_0 is the optical phonon energy.

The various matrix elements are calculated using the eigenvectors for the bands determined from the $\mathbf{k}\cdot\mathbf{p}$ method. To include the effects of the impurities in the highly doped emitter layers the energy of the light and heavy-hole bands is increased by a constant E_i. While this is not an exact correction to the bands, it gives reasonable results without greatly increasing the calculation time.

The carrier scattering rates for the various scattering processes are required for the transport and escape calculations. For the split-off band detectors three basic scattering processes need to be considered: (i) ionized impurity scattering, (ii) phonon scattering, and (iii) hot/cold carrier scattering.

The escape probability determination involves both the transport and scattering of the carriers as they move through the emitters to the interface and the actual escape of the carriers at the interface. At the interface the carrier either escapes, or is reflected based on the probabilities. There are two possible mechanisms for escape of the excited carriers. The first and dominant process is to directly escape over the barrier while remaining in the same hole band as presently occupied. This is the same process as in the HEIWIP detectors and the probability can be determined using an escape cone model [7,8] as has been done previously [9]. The second mechanism is for the carrier to scatter into a different band as it crosses the emitter/barrier interface for which the escape probability is calculated from the quantum mechanical transmission probability. The motion of the carrier is followed until it either escapes, or has energy less than the barrier when it is retained in the emitter.

3. Experimental

The initial tests on the effects of a graded barrier were performed using samples grown by two different approaches (superlattice and averaging) to the digital alloy technique. The first digital alloy approach is to consider the layers to behave in such a way that the carriers only see an average Al fraction for several adjacent layers. i.e., one monolayer of GaAs and two monolayers of AlAs would affect the carrier like three monolayers of $Al_{0.67}Ga_{0.33}As$. Under this approach high quality layers are actually a disadvantage as rough and partial layers will break up any superlattice effects. In the second approach, the layers act as a superlattice with the carriers being transported effectively in the ground state miniband. In this approach the effective barrier height will be determined by the ground state miniband at any given location. For this approach to be valid, the layer quality needs to be high with good interfaces so that the carrier wavefunctions are not localized in single wells.

Two sets of samples were grown using two different digital alloy approaches with a single emitter between a graded barrier and

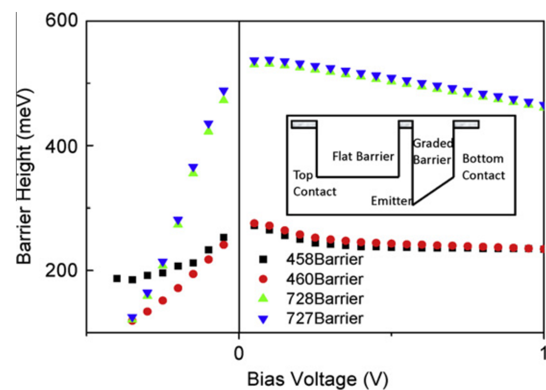

Fig. 1. The variation of the barrier height (calculated by Arrhenius plots using IVT data) with the bias voltage for the four structures. Notice the significant reduction in barrier height with bias under negative bias while the reduction is much less for positive bias. Inset: The band structure of the device with a graded barrier and a single emitter.

Author's personal copy

a constant barrier, as shown in inset of Fig. 1. One set of samples (458 and 460) was grown assuming the averaging approach with the constant barrier grown using non-digital techniques. The highest Al fraction at the graded barrier in this set of samples is 75%. The graded barrier was grown as 31 periods of GaAs and AlAs with thicknesses $(0.45 + 0.01\ N)L/31$ and $(0.55\text{–}0.01\ N)L/31$ respectively, where N is the number of the period and L is the total thickness of the graded barrier. The second set of samples (727 and 728) used the superlattice approach for both the graded and constant barriers. The graded barrier used 11.3 Å AlAs barriers throughout and 8, 9, 8, 9, and 8 periods, respectively of 6.4, 5.5, 4.6, 3.7 and 2.8 Å GaAs wells with a 118.9 Å AlAs barrier at the end. The constant barrier used 11.3 Å AlAs barriers and 6.5 Å GaAs wells. The highest Al fraction at the graded barrier in this set of samples is 100%. Both sets of samples were grown by MBE and mesa detectors were processed by wet etching and deposition of metal contact layers.

4. Results and discussion

Through IVT measurements, the highest operating temperature safe bias range, and the effective barrier height from, an Arrhenius plot were determined for each sample. The variation of barrier height with bias voltage is shown in Fig. 1. At negative bias i.e., when the top contact is negative, carriers will be injected at the graded barrier end, and positive bias is the reverse of this. To obtain the gain by reducing capture the bias should be negative. At low negative bias both samples show a rapid decrease due to the lowering of the graded barrier with bias. At low bias, the effective barrier is determined at the end of the graded barrier closest to the emitter. The carriers must have sufficient energy to pass over this end of the barrier after any energy relaxation which occurs in crossing the barrier. At sufficiently high bias, the end of the barrier adjacent to the contact will be higher than the end adjacent to the emitter and would then determine the effective barrier height. This can be seen as the slowly decreasing region for sample 458. For sample 727, only the low bias region is observed due to high currents. For positive bias, the effective barrier height is determined at low bias by the graded barrier which decreases with bias due to tunneling effects. At high positive biases, the graded barrier becomes less than the constant barrier so that the effective barrier is determined by the constant barrier which shows only a slow variation with bias. The difference in the extent of the decreasing region for positive bias between the two samples is due to the much larger barrier height of sample 727 compared to sample 458.

For samples 458 and 460, grown using the averaging approach, the barrier height under negative bias started at 280 meV and decreased to 175 meV at a bias of 0.35 V. Qualitatively, these results are as expected, however, the barrier heights observed were much less than the optimized heights of 400 and 235 meV at low and high bias respectively. The observed values match those expected from the energy levels in wells having the layer thicknesses used in the growth. This leads to the conclusion that although averaging effects expected, the sample had sufficiently high well quality to act as a superlattice. For positive bias, the maximum barrier was 280 meV decreasing to 240 meV at 0.3 V and 230 meV at 1.25 V. For the samples 727 and 728, grown using the superlattice approach, the effective barrier height starts at 500 meV for negative bias and decreases to 130 meV for a 0.4 V bias. However, for positive bias the barrier height also showed a significant decrease from 500 meV at 0.2 V to 250 meV at 3.2 V. Again the observed barrier heights under negative bias are significantly less than the optimized values of 530 and 300 meV at low and high bias respectively. However, on evaluating the layer parameters, it was noted that the GaAs layers in the graded barrier are very thin, less than a monolayer for much of the structure. This indicates that the sample is probably behaving according to the averaging model. The barrier heights from negative biases are also consistent with this interpretation.

These conclusions of the behavior of the barrier layers are supported by TEM measurements for the detectors. In Fig. 2 TEM images of the graded and constant barriers for sample 458 are shown. For the graded barrier region a good superlattice appearance is observed throughout the detector except for the topmost region of the barrier. Instead of observing 31 periods only 26 periods were seen. The reason for this is not clear as the GaAs layer thickness at this point should be 6.5–8.0 Å which would be visible based on the results for sample 727. The variation in thickness of the layers can be seen although precise quantitative results cannot be obtained due to the resolution limits of the image. The observed barrier height at low bias is consistent with the TEM image and should be the energy level in the narrowest well. The thicker AlAs layer would still be sufficiently thin for the carriers to tunnel through making its effects small on the predicted barrier. Removing this barrier would only shift the effective barrier height by $\sim$10 meV which is too small to be definitely identified. The constant barrier region is seen as a uniform layer with an expected barrier height of 240 meV. For sample 727 the TEM in Fig. 3 shows the layers with the thickness variation being observable. However, in this case the layers appear much more inconsistent and in some

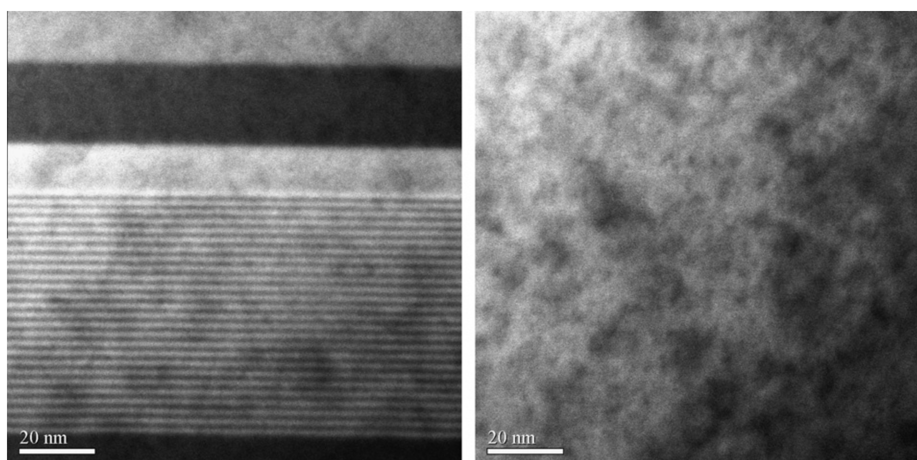

Fig. 2. The TEM images of the graded barrier and constant barrier regions for sample 458. Note the consistent layers in the graded barrier region, indicating superlattice behavior is expected. The constant barrier region shows no variations as it has no layers.

Author's personal copy

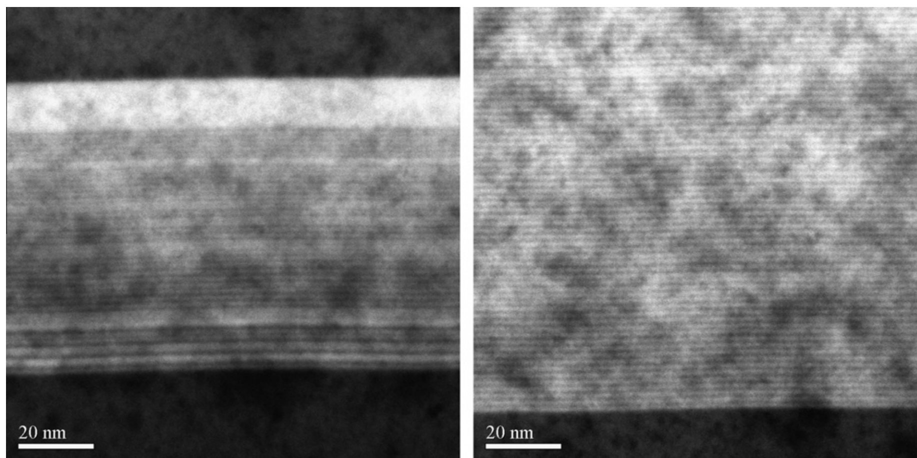

Fig. 3. The TEM images for the graded and constant barrier regions of sample 727. The layers are much less consistent than for sample 458 and there are layers in both the constant and graded barrier regions. This sample should behave as if the layers are averaged.

regions appear to almost disappear supporting the conclusion that this sample is behaving according to the averaging model. This same behavior is observed in the constant barrier region for this sample.

The carrier transport and effective barrier height are shown in Fig. 4. For sample 458, the carriers are transported directly from well to well in the digital alloy of the graded barrier with an effective barrier height determined by the ground state energy in the wells. At higher temperature tunneling can occur into the second or third well reducing the effective barrier height for dark current. For sample 727, the average composition determines the transport with the carriers moving as if over the top of the trapezoidal barrier. As a result of these effects the effective barrier height for sample 458 was reduced while the barrier height of sample 727 was increased as can be seen from Fig. 1 where barrier for sample 727 is much higher for sample 458, while sample 458 does not show the expected high barrier at low biases.

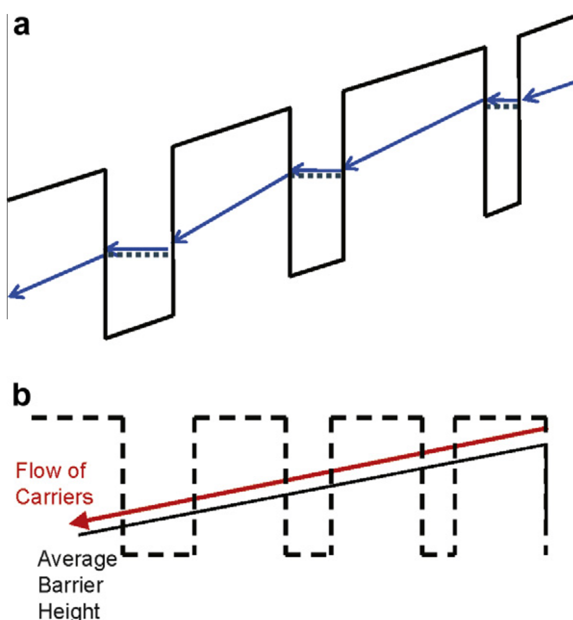

Fig. 4. (a) The carriers in 458 are transported directly from well to well in the digital alloy of the graded barrier with an effective barrier height determined by the ground state energy in the wells. At higher temperature tunneling can occur into the second or third well reducing the effective barrier height. (b) For sample 727, the average composition determines the transport with the carriers moving as if over the top of the trapezoidal barrier.

For sample 460, the barrier was lower than the split-off energy so both free carrier and split-off responses were observed as seen in Fig. 5. In this detector most of the response is observed from the emitter with the contact layer contributing only a small fraction. This is due to the similarity of the barriers on both of the emitter 280 and 240 meV based on the Arrhenious data. This leads to a large capture rate for injected carriers and reduces the gain from the detector. Another significant feature observed in the response of this detector is the very different response levels observed under forward and reverse bias. Switching the polarity of the bias leads to a three order of magnitude change in the response at 150 K. This is believed to be due to the depletion of the emitter under positive bias at this temperature. The thermally excited carriers can much more easily tunnel out of the emitter than they can enter the constant barrier over the top. This depletion leads to most of the applied field being across the constant barrier at positive bias and hence a reduced response. This effect is reduced at 80 K where the response under forward and reversed bias differs by less than a factor of two. The reduction in this effect is due to the greatly reduced thermally assisted tunneling at the lower temperature.

The spectral response for sample 728 is shown in Fig. 6, the response under negative bias is observed only at low bias values, as

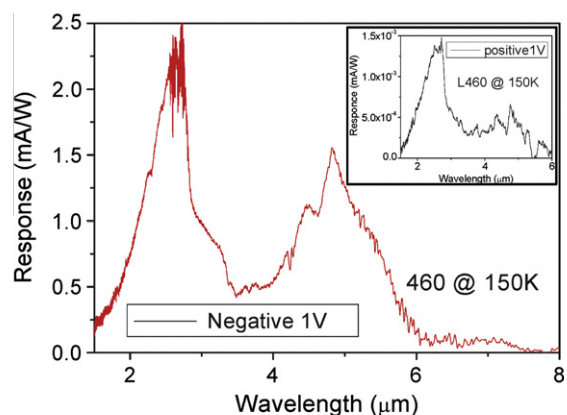

Fig. 5. The spectral response of 460 at 150 K. There is a great difference between the forward and reverse bias responses. In this detector both free carrier and split-off responses can be seen.

Author's personal copy

the safe current limit reach it very low bias. Under these conditions, the Arrhenious data indicates the emitter is depleted, so that the response will be primarily from the bottom contact. Since the split-off energy is much less than the effective barrier height, the response is due to free-carrier absorption. For positive bias, the carriers are all trapped at the emitter.

The detectivity of the samples 460 and 728 are 9.2×10^5 Jones, and 2.2×10^2 Jones respectively at their operating temperatures. Although the results of these detectors do not show the desired improvements they do indicate possible methods of improving the detectors, an optimized device will have much higher D*, in the range 10^{10}–10^{11} Jones.

While samples 458 and 460, which behaved as a superlattice, gave reasonable results, although the barrier was not sufficiently high to obtain a high temperature response, the best response was observed at 150 K. Narrowing the well to obtain the desired ground state did not work as it led to the wells being too thin for good quality as was observed in sample 727, even though they give a response around room temperature the response is very weak. This indicates that any future attempts using a digital alloy should use the averaging approach, but the layers should be thinner than were used in sample 458 to give an improved averaging behavior. The samples also showed that the introduction of the barrier offset does affect the relationship between the trapping and escape of carriers in the emitter. For sample 727 under negative bias, the sample behaved as the total bias drop occurred across the graded barrier. This indicates that trapping is very low in this sample and the emitter is depleted. In sample 458 however, the bias drop is divided between the two barriers. This indicates that trapping and escape are much more nearly balanced in this sample as is desired in an optimized detector. These results indicate that it is possible to adjust the trapping with barrier offset and an optimized design should give an improved response. Based on the results of these samples, an optimized single emitter design would use a single graded barrier with 60 nm thickness graded from $x = 0.45$ to 0.75, a 80 nm thick GaAs emitter doped to 1×10^{19} cm^{-3} and a 400 nm thick $Al_{0.57}Ga_{0.43}As$ barrier. The expected response and specific detectivity D* comparison with and without the graded barrier is shown in Fig. 7. The graded barrier leads to almost two orders of magnitude improvement in the response.

As a result of hole transitions between the light-hole and heavy-hole bands, p-GaAs is able to show the optical absorption in the spectral range above the split-off absorption. The long-wavelength response as shown in Fig. 8a was measured on detector SP1 which consists of 30 periods of p-GaAs emitters doped to 3.0×10^{18} cm^{-3} and constant $Al_{0.28}Ga_{0.72}As$ barriers. In comparison with the calculated free-carrier response using an escape model, the light-hole and heavy-hole band transitions contribute to the 4–8 μm response range. At high bias, the detector shows a response up to ~10 μm, whereas, response longer than 10 μm was observed with the increasing of temperature as shown in Fig. 8b. This feature could be due to the thermal detection mechanisms. The absorption efficiency was calculated to show the cavity enhancement of the

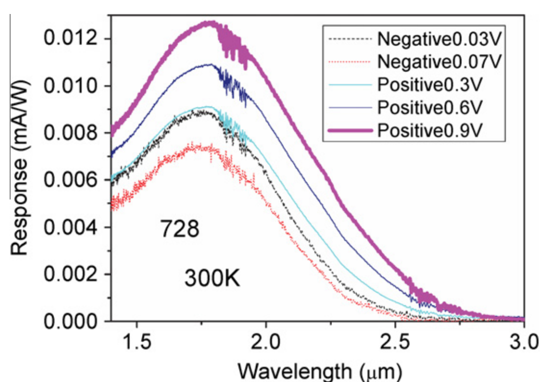

Fig. 6. The spectral response of 728 at 300 K. Here only a free-carrier response is observed due to the barrier being above the split-off energy.

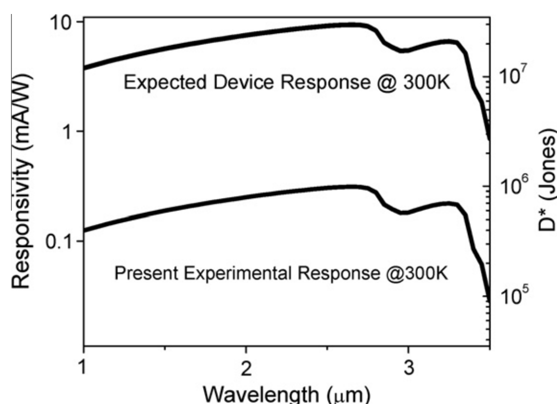

Fig. 7. The theoretically expected responsivity at different wavelengths with and without the graded barrier with a barrier offset.

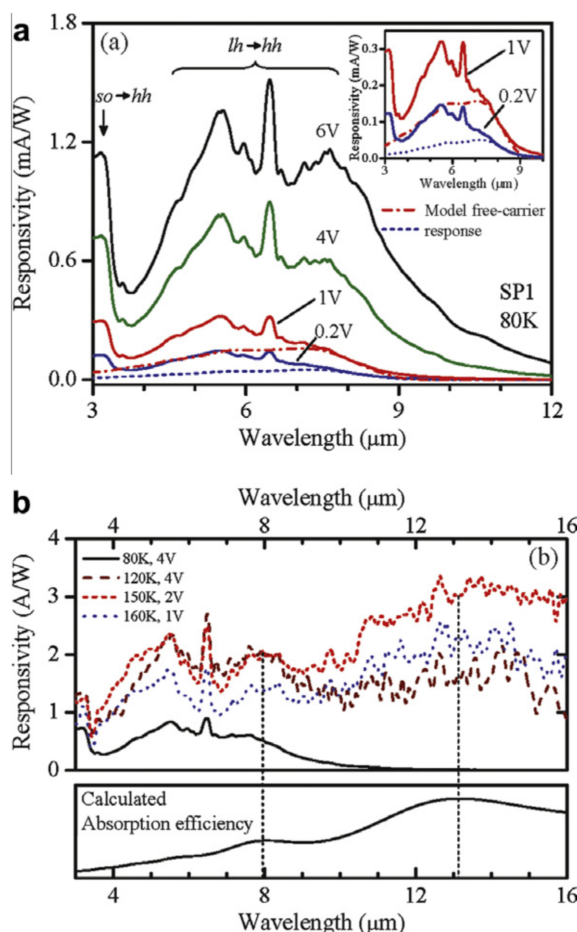

Fig. 8. (a) The 80 K responsivity spectra of detector SP1 at different bias. The inset shows the comparison with modeled free-carrier responsivity indicating the 4–8 μm response range is due to the light-hole and heavy-hole band transitions. (b) Response spectra of SP1 at different temperatures. The wavelength region above 10 μm is due to a thermal detection mechanism. Calculated absorption efficiency shows the cavity enhancement effects.

Author's personal copy

p-GaAs/AlGaAs structure which leads to peaks at 7.9 and 13 μm. These results will be useful for designing multi-spectral detection including mid- and long-wavelength infrared range by using a single p-type GaAs-based structure.

Acknowledgments

This work supported by the US Army research office under Grant No. W911NF-08-1-0448, monitored by Dr. William W. Clark and a grant from the EPSRC (UK).

References

[1] G. Ariyawansa, A.G.U. Perera, X.H. Su, S. Chakrabarti, P. Bhattacharya, Multicolor tunneling quantum dot infrared photodetectors operating at room temperature, Infrared Phys. Technol. 50 (2007) 156–161.

[2] H.S. Kim et al., Mid-IR focal plane array based on type-II InAs/GaSb strain layer superlattice detector with nBn design, Appl. Phys. Lett. 92 (2008) 183502–183503.

[3] A.G.U. Perera, S.G. Matsik, P.V.V. Jayaweera, K. Tennakone, H.C. Liu, M. Buchanan, G. Von Winckel, A. Stintz, S. Krishna, High operating temperature split-off band infrared detectors, Appl. Phys. Lett. 89 (2006) 131118–131123.

[4] P.V.V. Jayaweera, S.G. Matsik, A.G.U. Perera, H.C. Liu, M. Buchanan, Z.R. Wasilewski, Uncooled infrared detectors for 3–5 μm and beyond, Appl. Phys. Lett. 93 (2008) 021105–021113.

[5] Y. Lao, P.K.D.D.P. Pitigala, A.G.U. Perera, H.C. Liu, M. Buchanan, Z.R. Wasilewski, K.K. Choi, P. Wijewarnasuriya, Light-hole and heavy-hole transitions for high-temperature long-wavelength infrared detection, Applied Physics Letters 97 (2010) 091104–091103.

[6] K. Seeger, in: Semiconductor Physics, fifth ed., Springer–Verlag, 1991. chapter 6.

[7] V.E. Vickers, Model of Schottky barrier hot-electron-mode Photodetection, Appl. Opt. 10 (1971) 2190–2192.

[8] J.M. Mooney, J. Silverman, The theory of hot-electron photoemission in Schottky-barrier IR detectors, IEEE Trans. Electron Devices 32 (1985) 33–39.

[9] G. Ariyawansa, V. Apalkov, A.G.U. Perera, S.G. Matsik, G. Huang, P. Bhattacharya, Bias-selectable tricolor tunneling quantum dot infrared photodetector for atmospheric windows, Appl. Phys. Lett. 92 (2008) 111104–111113.